

# CEDNET: A CASCADE ENCODER-DECODER NETWORK FOR DENSE PREDICTION

Gang Zhang<sup>1</sup>, Ziyi Li<sup>4</sup>, Chufeng Tang<sup>1</sup>, Jianmin Li<sup>1</sup>, Xiaolin Hu<sup>1,2,3\*</sup>

<sup>1</sup>Department of Computer Science and Technology, Institute for AI, BNRist, THU-Bosch JCML Center, Tsinghua University, Beijing 100084, China

<sup>2</sup>Tsinghua Laboratory of Brain and Intelligence (THBI), IDG/McGovern Institute for Brain Research, Tsinghua University, Beijing 100084, China

<sup>3</sup>Chinese Institute for Brain Research (CIBR), Beijing 100010, China

<sup>4</sup>Huazhong University of Science and Technology, Wuhan 430074, China

{zhang-g19,tcf18}@mails.tsinghua.edu.cn, liziyi@hust.edu.cn,

{lijianmin,xlhu}@mail.tsinghua.edu.cn

Code: <https://github.com/zhanggang001/CEDNet>

## ABSTRACT

Multi-scale features are essential for dense prediction tasks, such as object detection, instance segmentation, and semantic segmentation. The prevailing methods usually utilize a classification backbone to extract multi-scale features and then fuse these features using a lightweight module (*e.g.*, the fusion module in FPN and BiFPN, two typical object detection methods). However, as these methods allocate most computational resources to the classification backbone, the multi-scale feature fusion in these methods is delayed, which may lead to inadequate feature fusion. While some methods perform feature fusion from early stages, they either fail to fully leverage high-level features to guide low-level feature learning or have complex structures, resulting in sub-optimal performance. We propose a streamlined cascade encoder-decoder network, dubbed CEDNet, tailored for dense prediction tasks. All stages in CEDNet share the same encoder-decoder structure and perform multi-scale feature fusion within the decoder. A hallmark of CEDNet is its ability to incorporate high-level features from early stages to guide low-level feature learning in subsequent stages, thereby enhancing the effectiveness of multi-scale feature fusion. We explored three well-known encoder-decoder structures: Hourglass, UNet, and FPN. When integrated into CEDNet, they performed much better than traditional methods that use a pre-designed classification backbone combined with a lightweight fusion module. Extensive experiments on object detection, instance segmentation, and semantic segmentation demonstrated the effectiveness of our method. The code has been released.

## 1 INTRODUCTION

In recent years, both convolutional neural networks (CNNs) and transformer-based networks have achieved remarkable results in various computer vision tasks, including image classification, object detection, and semantic segmentation. In image classification, the widely-used CNNs (Krizhevsky et al., 2012; Simonyan & Zisserman, 2015; Szegedy et al., 2015; He et al., 2016; Liu et al., 2022) as well as the recently developed transformer-based networks (Liu et al., 2021; Yang et al., 2021; Dong et al., 2022; Zhang et al., 2023b) generally follow a sequential architectural design. They progressively reduce the spatial size of feature maps and make predictions based on the coarsest scale of features. However, in dense prediction tasks, such as object detection and instance segmentation, the need for multi-scale features arises to accommodate objects of diverse sizes. Therefore, effectively extracting and fusing multi-scale features becomes essential for the success of these tasks (He et al., 2017; Lin et al., 2017b; Tian et al., 2019; Xiao et al., 2018; Zhang et al., 2021; Hu et al., 2022).

---

\*Corresponding Author

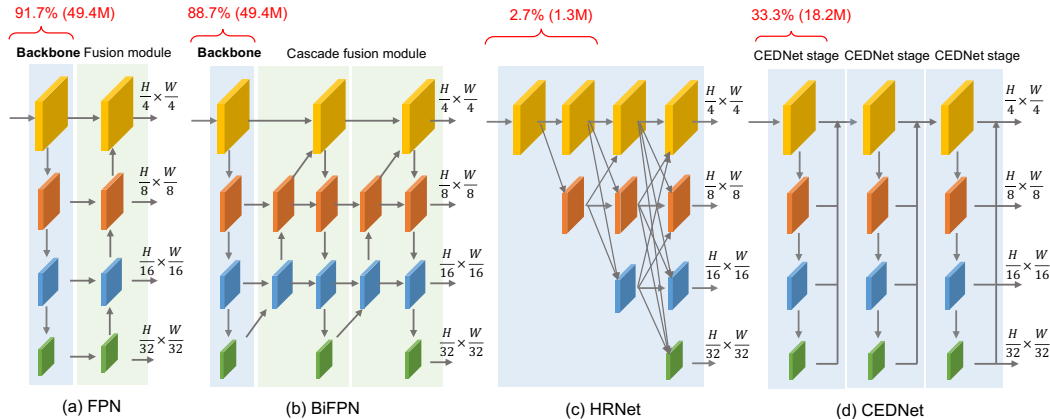


Figure 1: Comparison among FPN, BiFPN, HRNet, and our CEDNet.  $H \times W$  denotes the spatial size of the input image. At the top of each panel, the percentage indicates the time to perform the first multi-scale feature fusion, while the number in bracket is the number of parameters of the selected part. For these calculations, we take ConvNeXt-S as the backbone of FPN and BiFPN. While we illustrate a CEDNet of four scales here for a clearer comparison, it’s noteworthy that in our actual implementation, feature maps with a resolution of  $\frac{H}{4} \times \frac{W}{4}$  are not included in the CEDNet stages.

Many methods have been proposed for multi-scale feature extraction and fusion (Lin et al., 2017a; Liu et al., 2018; Ghiasi et al., 2019; Tan et al., 2020). One widely-used model is the feature pyramid network (FPN) (Lin et al., 2017a) (Figure 1 (a)). FPN consists of a pre-designed classification backbone for extracting multi-scale features and a lightweight fusion module for fusing these features. Moving beyond the FPN, some cascade fusion strategies have been developed and showcased efficacy in multi-scale feature fusion (Liu et al., 2018; Ghiasi et al., 2019; Tan et al., 2020). Figure 1 (b) shows the structure of the representative BiFPN (Tan et al., 2020). It iteratively fuses multi-scale features using repeated bottom-up and top-down pathways. However, the time for feature fusion in these networks is relatively late, because they allocate most computational resources to the classification backbone to extract the initial multi-scale features. We define *the time for feature fusion* as the ratio of the parameters of the sub-network before the first fusion module to the whole network. A smaller ratio indicates an earlier time. For instance, considering an FPN built based on the classification model ConvNeXt-S (Liu et al., 2022), the time for feature fusion is the ratio of the parameters of the backbone ConvNeXt-S to the entire FPN (91.7%). Given the complexity of dense prediction tasks where models are required to handle objects of diverse sizes, we expect that integrating early multi-scale feature fusion within the backbone could enhance model performance.

Some methods have transitioned from using pre-designed classification networks to designing task-specific backbones for dense prediction tasks (Wang et al., 2019; Du et al., 2020; Jiang et al., 2022; Cai et al., 2023). In these methods, some incorporate early multi-scale feature fusion. For example, HRNet (Wang et al., 2019), one of the representative works (Figure 1 (c)), aims to learn semantically rich and spatially precise features. Although HRNet performs the first feature fusion very early (2.7%), it generates high-level (low-resolution) features with strong semantic information quite late. This limits their role in guiding the learning of low-level (high-resolution) features that are important for dense prediction tasks. In contrast, SpineNet (Du et al., 2020) employs neural architecture search (NAS) (Zoph & Le, 2017) to learn a scale-permuted backbone with early feature fusion. Nevertheless, the resulting network is complex and exhibits limited performance when transferred to different detectors (Du et al., 2020). GiraffeDet (Jiang et al., 2022) integrates a lightweight backbone with a heavy fusion module for object detection, aiming to enhance the information exchange between high-level and low-level features. Yet, it fuses multi-scale features in a fully connected way, which inevitably increases runtime latency. A detailed discussion of related works can be found in Section 2.2. Clearly, an appropriate structure for effective early multi-scale feature fusion is lacking.

In this paper, we present CEDNet, a cascade encoder-decoder network tailored for dense prediction tasks. CEDNet begins with a stem module to extract initial high-resolution features. Following this, CEDNet incorporates several cascade stages to generate multi-scale features, with all stages sharing the same encoder-decoder structure. The encoder-decoder structure can be realized in various ways.

Figure 1 (d) illustrates a three-stage CEDNet built on the FPN-style design. CEDNet evenly allocates its computational resources across stages and fuses multi-scale features within each decoder. As a result, CEDNet performs multi-scale feature fusion from the early stages of the network. This strategy ensures that high-level features from the early stages are integrated to guide the learning of low-level features in subsequent stages. Moreover, CEDNet possesses a more streamlined and efficient structure, making it suitable for a wide variety of models and tasks.

We investigated three well-known methods, *i.e.*, Hourglass (Newell et al., 2016), UNet (Ronneberger et al., 2015), and FPN (Ghiasi et al., 2019), as the encoder-decoder structure in experiments and found that they all performed well. Due to the slightly better results of the FPN, it is adopted as the default encoder-decoder structure in CEDNet for further analysis on object detection, instance segmentation and semantic segmentation. On the COCO *val 2017* for object detection and instance segmentation, the CEDNet variants outperformed their counterparts, *i.e.*, the ConvNeXt variants (Liu et al., 2022), achieving an increase of 1.9-2.9 % in box AP and 1.2-1.8% in mask AP based on the popular framework RetinaNet (He et al., 2016) and Mask R-CNN (He et al., 2017). On the ADE20k for semantic segmentation, the CEDNet variants outperformed their counterparts by 0.8-2.2% mIoU based on the renowned framework UperNet (Xiao et al., 2018). These results demonstrate the excellent performance of CEDNet and encourage the community to rethink the prevalent model design principle for dense prediction tasks.

## 2 RELATED WORK

### 2.1 MULTI-SCALE FEATURE FUSION

Many methods adopt pre-designed classification backbones to extract multi-scale features. However, the low-level features produced by traditional classification networks are semantically weak and ill-suited for downstream dense prediction tasks. To tackle this limitation, many strategies (Lin et al., 2017a; Liu et al., 2018; Tan et al., 2020; Chen et al., 2018; Ghiasi et al., 2019) have been proposed for multi-scale feature fusion. In semantic segmentation, DeeplabV3+ (Chen et al., 2018) fuses low-level features with semantically strong high-level features produced by atrous spatial pyramid pooling. In object detection, FPN (Lin et al., 2017a) introduces a top-down pathway to sequentially combine high-level features with low-level features. NAS-FPN (Ghiasi et al., 2019) fuses multi-scale features by repeated fusion stages searched by neural architecture search (Zoph & Le, 2017). EfficientDet (Tan et al., 2020) adopts a weighted bi-directional feature pyramid network in conjunction with a compound scaling rule to achieve efficient feature fusion. A common drawback of these methods is that they allocate most computational resources to the classification backbone, delaying feature fusion and potentially undermining fusion effectiveness. In contrast, our approach evenly allocates computational resources to multiple stages and perform feature fusion within each stage.

### 2.2 BACKBONE DESIGNS FOR DENSE PREDICTION

Instead of fusing multi-scale features from pre-designed classification networks, some studies have attempted to design task-specific backbones for dense prediction tasks (Ronneberger et al., 2015; Newell et al., 2016; Wang et al., 2019; Du et al., 2020; Jiang et al., 2022; Liu et al., 2020; Qiao et al., 2021; Cai et al., 2023). For instance, UNet (Ronneberger et al., 2015) employs a U-shape structure to acquire high-resolution and semantically strong features in medical image segmentation. Hourglass (Newell et al., 2016) introduces a convolutional network consisting of repeated bottom-up and top-down pathways for human pose estimation. HRNet (Wang et al., 2019) retains high-resolution features throughout the whole network and performs well in semantic segmentation and human pose estimation. In object detection, SpineNet (Du et al., 2020) leverages neural architecture search (Zoph & Le, 2017) to learn scale-permuted backbones. GiraffeDet (Jiang et al., 2022) pairs a lightweight backbone with a heavy fusion module to encourage dense information exchange among multi-scale features. RevCol (Cai et al., 2023) feeds the input image to several identical subnetworks simultaneously and connects them through reversible transformations.

While the aforementioned methods incorporate early multi-scale feature fusion, they either exhibit effectiveness solely on specific models and tasks (Ronneberger et al., 2015; Newell et al., 2016; Du et al., 2020), or do not fully harness the potential of high-level features to guide the learning of low-level features (Wang et al., 2019; Cai et al., 2023). In contrast, our method incorporates multiple

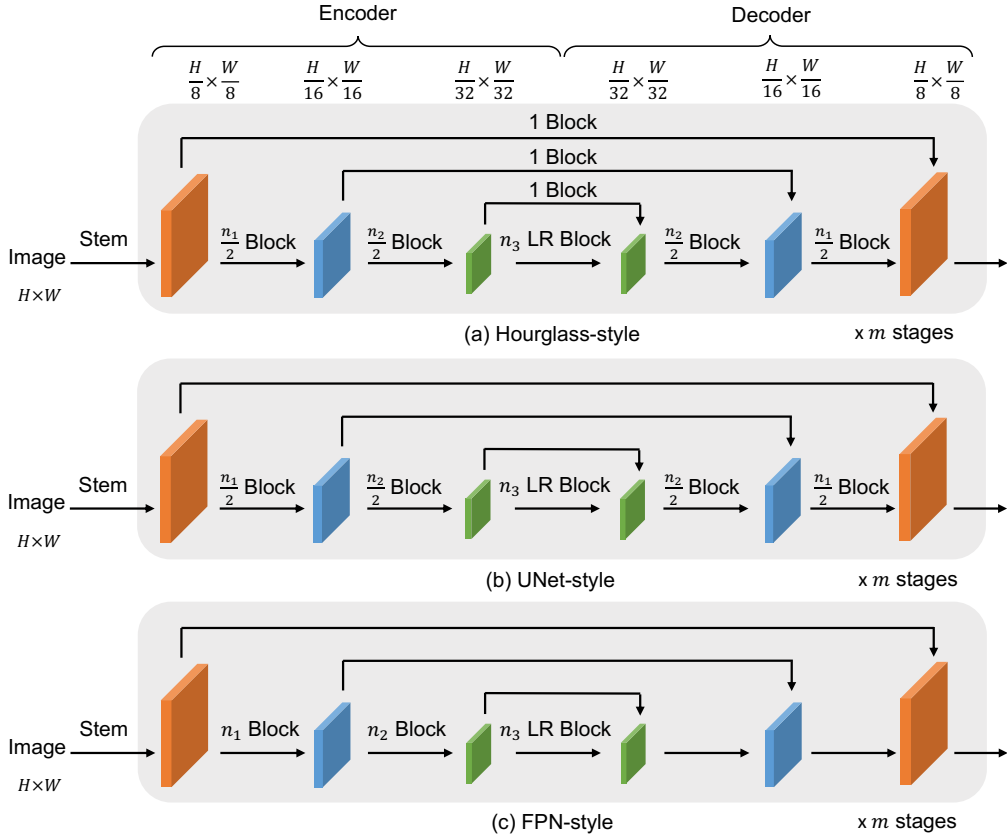


Figure 2: Three implementations of CEDNet. The input image with a spatial size of  $H \times W$  is fed into a lightweight stem module to extract high-resolution features of size  $\frac{H}{8} \times \frac{W}{8}$ . These features are then processed through  $m$  cascade stages to extract multi-scale features. Block denotes CED block, and LR Block denotes long-range (LR) CED block. The down-sampling layers ( $2 \times 2$  convolution with stride 2) and the up-sampling layers (bilinear interpolation) are omitted for clarity.

cascade stages to iteratively extract and fuse multi-scale features. Therefore, the high-level features from early stages can be integrated to instruct the learning of low-level features in subsequent stages. Moreover, CEDNet showcases excellent performance across a broad spectrum of models and tasks.

### 3 CEDNET

#### 3.1 OVERALL ARCHITECTURE

Figure 2 illustrates the overall architecture of CEDNet. The input RGB image with a spatial size of  $H \times W$  is fed into a stem module to extract high-resolution feature maps of size  $\frac{H}{8} \times \frac{W}{8}$ . The stem module comprises two sequential  $3 \times 3$  convolutional layers (each with a stride of 2),  $n_0$  CED blocks, and a  $2 \times 2$  convolutional layer with a stride of 2. Each  $3 \times 3$  convolutional layer is followed by a LayerNorm (Ba et al., 2016) layer and a GELU (Hendrycks & Gimpel, 2016) unit. The further details about the CED block can be found in Section 3.3. Subsequently,  $m$  cascade stages, each with the same encoder-decoder structure, are utilized to extract multi-scale features. The multi-scale features from the final decoder are then fed into downstream dense prediction tasks. *Unlike in FPN and BiFPN, no extra feature fusion modules are required after the CEDNet backbone.* We discuss three implementations of the encoder-decoder structure in Section 3.2.

#### 3.2 THREE ENCODER-DECODER STRUCTURES

In CEDNet, each stage employs an encoder-decoder structure. The encoder extracts multi-scale features, while the decoder integrates these features into single-scale, highest-resolution ones. Conse-

quently, the high-level (low-resolution) features from early stages are integrated to guide the learning of low-level features in subsequent stages. While many methods can be used to realize the encoder-decoder structure, we adopt three well-known methods for our purposes in this study.

**Hourglass-style.** The Hourglass network (Newell et al., 2016) is a deep learning architecture specifically designed for human pose estimation. It resembles an encoder-decoder design but stands out with its symmetrical hourglass shape, from which its name is derived. In this study, we draw inspiration from the Hourglass architecture to devise an hourglass-style encoder-decoder (Figure 2 (a)). In alignment with the original design, a CED block is employed to transform the feature maps from the encoder before integrating them into the symmetrical feature maps in the decoder.

**UNet-style.** UNet is a prominent network primarily employed in medical image segmentation (Ronneberger et al., 2015). Recent advancements have also shown its successful application in diffusion models (Zhang et al., 2023a). As illustrated in Figure 2 (b), the UNet-style encoder-decoder has a symmetrical shape. Unlike the hourglass-style design, identity skip connections are harnessed to bridge the symmetrical feature maps between the encoder and the decoder.

**FPN-style.** FPN (Lin et al., 2017a) is initially designed for object detection and instance segmentation, aiming to fuse multi-scale features from pre-designed classification networks. In this work, we incorporate the FPN-style encoder-decoder as a separate stage in CEDNet, as shown in Figure 2 (c). Different from the standard FPN implementation, we eliminate the  $3\times 3$  convolutions responsible for transforming the merged symmetrical feature maps. As a result, most computational resources are allocated to the encoders, with only two  $1\times 1$  convolutions in each decoder for feature channel alignment.

### 3.3 BLOCK DESIGNS

**CED block.** The *solid elements* in Figure 3 illustrate the general structure of the CED block. This block comprises a token mixer for spatial feature interactions and a multi-layer perceptron (MLP) with two layers for channel feature interactions. The token mixer can be various existing designs, such as the  $3\times 3$  convolution in ResNet (He et al., 2016), the  $7\times 7$  depth-wise convolution in ConvNeXt (Liu et al., 2022), and the local window attention in Swin transformer (Liu et al., 2021). In CEDNet, we take the lightweight  $7\times 7$  depth-wise convolution from ConvNeXt as the default token mixer. *Please note that a more powerful token mixer may yield enhanced performance, but that is not the focus of this work.*

**LR CED block.** To increase the receptive field of neurons, we introduce the LR CED block. Beyond the CED block, this block incorporates a  $7\times 7$  *dilated* depth-wise convolution accompanied by two skip connections, as highlighted by the dashed elements. By integrating the dilated depth-wise convolution, the LR CED block is capable of capturing long-range dependencies among spatial features with only a marginal increase in parameters and computational overhead. The LR CED blocks are utilized to transform the lowest-resolution features in each CEDNet stage.

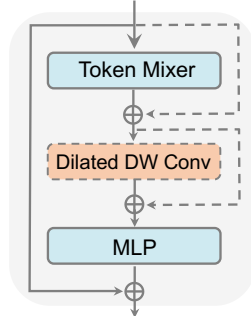


Figure 3: Structure of the CED block and the LR CED block. The CED block consists solely of solid elements, while the LR CED block includes both solid and dashed elements. DW Conv is short for depth-wise convolution.

### 3.4 ARCHITECTURE SPECIFICATIONS

We have constructed three CEDNet variants based on the FPN-style encoder-decoder, *i.e.*, CEDNet-NeXt-T/S/B, where the suffixes T/S/B indicate the model size tiny/small/base. We take the  $7\times 7$  depth-wise convolution from ConvNeXt as the default token mixer for all (LR) CED blocks. For all LR CED blocks, we set the dilation rate  $r$  of the dilated convolution to 3. These variants adopt different channel dimensions  $C$ , different numbers of blocks  $B = (n_0, n_1, n_2, n_3)$ , and different numbers of stages  $m$ . The configuration hyper-parameters for these variants are presented below:

- CEDNet-NeXt-T:  $C=(96, 192, 352, 512)$ ,  $B=(3, 2, 4, 2)$ ,  $m=3$
- CEDNet-NeXt-S:  $C=(96, 192, 352, 512)$ ,  $B=(3, 2, 7, 2)$ ,  $m=4$
- CEDNet-NeXt-B:  $C=(128, 256, 448, 704)$ ,  $B=(3, 2, 7, 2)$ ,  $m=4$

Table 1: Comparison among three encoder-decoder structures.  $AP^b$  is the overall detection accuracy on COCO *val2017*. The model inference speed FPS was measured on a single RTX 3090 GPU.

Method	Param	FLOPs	$AP^b$	$AP_{50}^b$	$AP_{75}^b$	FPS $\uparrow$
ConvNeXt-T w/ FPN (Lin et al., 2017a)	39M	243G	45.4	66.5	48.7	20.0
ConvNeXt-T w/ NAS-FPN (Ghiasi et al., 2019)	47M	289G	46.6	66.8	49.9	18.1
ConvNeXt-T w/ BiFPN Tan et al. (2020)	39M	248G	46.7	67.1	50.2	16.8
HRNet-w32 (Wang et al., 2019)	39M	320G	45.7	66.5	49.2	15.9
SpineNet-96 (Du et al., 2020)	43M	265G	47.1	67.1	51.1	16.3
GiraffeDet-D11 (Jiang et al., 2022)	69M	275G	46.6	65.0	51.1	12.4
CEDNet-NeXt-T (Hourglass-style)	39M	255M	47.4	68.5	50.7	15.9
CEDNet-NeXt-T (UNet-style)	39M	255M	47.9	68.9	51.4	16.7
CEDNet-NeXt-T (FPN-style)	39M	255M	<b>48.3</b>	<b>69.1</b>	<b>51.6</b>	17.1

## 4 EXPERIMENTS

### 4.1 THREE ENCODER-DECODER STRUCTURES

We conducted experiments to compare the three encoder-decoder structures.

**Pre-training settings.** Following common practice (Liu et al., 2021; 2022), we pre-trained CEDNet on the ImageNet-1K dataset (Deng et al., 2009). The ImageNet-1K dataset consists of 1000 object classes with 1.2M training images. To perform classification, we removed the last decoder and attached a classification head on the lowest-resolution features from the last stage. The hyperparameters, augmentation and regularization strategies strictly follows (Liu et al., 2022).

**Pre-training results.** We built the CEDNet models using three different encoder-decoder structures. Appendix A presents the results of the CEDNet models on ImageNet-1K in comparison with some recent methods in image classification. We report the top-1 accuracy on the validation set. Table A1 shows that the CEDNet models slightly outperformed their counterparts, *i.e.*, the ConvNeXt variants. *Please note that the CEDNet is specifically designed for dense prediction tasks, and surpassing state-of-the-art methods in image classification is not our goal.*

**Fine-tuning settings.** We fine-tuned models on object detection with COCO 2017 (Lin et al., 2014) based on the well-known detection framework RetinaNet (Lin et al., 2017b) using the MMDetection toolboxes (Chen et al., 2019). For training settings, we mainly followed (Liu et al., 2022). Additionally, we found that the proposed CEDNet models were easy to overfit the training data. To fully explore the potential of CEDNet models, we used large scale jittering and copy-and-paste data augmentation following (Ghiasi et al., 2021), but only with box annotations. We re-trained all baseline models with the same data augmentation for a fair comparison.

**Fine-tuning results.** Table 1 shows that all three CEDNet models yielded significant gains over the models with FPN, NAS-FPN, and BiFPN, all of which utilize the classification network ConvNeXt-T to extract initial multi-scale features. This result validates the effectiveness of the cascade encoder-decoder network that performs multi-scale feature fusion from early stages. In addition, the CEDNet models surpassed other early feature fusion methods: HRNet, SpineNet, and GiraffeDet. We attempted to pre-train the entire BiFPN model by attaching a classification head to the coarsest feature maps of the last bottom-up pathway in the fusion module. However, we obtained poor results, *i.e.*, 76.8% top-1 accuracy on ImageNet and 39.4% box AP on COCO.

Since the model built on the FPN-style encoder-decoder slightly outperformed the models built on the UNet-style and Hourglass-style encoder-decoder in both detection accuracy and model inference speed, *we adopted the FPN-style encoder-decoder for CEDNet by default in subsequent experiments.*

### 4.2 OBJECT DETECTION ON COCO

**Settings.** We benchmark our models on object detection with COCO 2017 (Lin et al., 2014) based on four representative frameworks, *i.e.*, Deformable DETR (Zhu et al., 2021), RetinaNet (Lin et al.,

Table 2: Results of object detection and instance segmentation on the COCO *val2017*.  $AP^b$  and  $AP^m$  are the overall metrics for object detection and instance segmentation, respectively. If required, FPN was adopted as the default fusion module for methods except CEDNet and the models marked by  $\dagger$

(a) Deformable DETR								
Method	Param	FLOPs	$AP^b$	$AP^b_{50}$	$AP^b_{75}$	$AP^b_S$	$AP^b_M$	$AP^b_L$
ConvNeXt-T	42M	231G	47.1	66.7	51.8	28.8	50.5	62.3
ConvNeXt-S	64M	317G	49.0	68.6	53.7	31.2	52.4	64.5
CEDNet-NeXt-T	43M	223G	49.3	69.1	53.7	32.1	52.8	65.3
CEDNet-NeXt-S	65M	304G	50.3	70.2	55.2	32.3	54.6	65.2
(b) RetinaNet								
Backbone	Param	FLOPs	$AP^b$	$AP^b_{50}$	$AP^b_{75}$	$AP^b_S$	$AP^b_M$	$AP^b_L$
SpineNet-143 $\dagger$ (Du et al., 2020)	67M	524G	48.1	67.6	52.0	30.2	51.1	59.9
Swin-T (Liu et al., 2021)	39M	245G	45.0	65.9	48.4	29.7	48.9	58.1
Swin-S (Liu et al., 2021)	60M	335G	46.4	67.0	50.1	31.0	50.1	60.3
Swin-B (Liu et al., 2021)	98M	477G	45.8	66.4	49.1	29.9	49.4	60.3
ConvNeXt-T	39M	243G	45.4	67.0	48.7	29.5	49.9	59.9
ConvNeXt-S	60M	329G	47.4	68.3	51.2	32.0	51.5	61.6
CEDNet-NeXt-T	39M	255G	48.3	69.1	51.6	33.2	53.1	62.7
CEDNet-NeXt-S	61M	335G	49.6	70.8	53.2	34.8	54.0	63.5
(c) Mask R-CNN								
Backbone	Param	FLOPs	$AP^b$	$AP^b_{50}$	$AP^b_{75}$	$AP^m$	$AP^m_{50}$	$AP^m_{75}$
DetectoRS-50 $\dagger$ (Qiao et al., 2021)	105M	432G	46.2	65.1	50.2	40.4	62.5	43.5
Swin-T (Liu et al., 2021)	48M	264G	46.0	68.1	50.3	41.6	65.1	44.9
Swin-S (Liu et al., 2021)	69M	354G	48.5	70.2	53.5	43.3	67.3	46.6
FocalNet-S (Yang et al., 2022)	72M	365G	49.3	50.9	54.6	44.1	67.9	47.4
Swin-B (Liu et al., 2021)	107M	496G	48.5	69.8	53.2	43.4	66.8	46.9
FocalNet-B (Yang et al., 2022)	114M	507G	49.8	70.7	54.2	43.8	68.2	47.2
ConvNeXt-T	48M	262G	46.4	68.1	51.3	42.3	65.2	45.9
ConvNeXt-S	70M	348G	48.5	70.0	53.3	43.8	67.2	47.7
CEDNet-NeXt-T	49M	274G	49.2	70.3	53.7	44.1	67.8	47.5
CEDNet-NeXt-S	72M	355G	50.4	71.7	55.1	45.0	68.9	48.6
(d) Cascade Mask R-CNN								
Backbone	Param	FLOPs	$AP^b$	$AP^b_{50}$	$AP^b_{75}$	$AP^m$	$AP^m_{50}$	$AP^m_{75}$
CBNet-X152 (Liu et al., 2020)	238M	1358G	50.7	69.8	55.5	43.3	66.9	46.8
Swin-T (Liu et al., 2021)	86M	745G	50.5	69.3	54.9	43.7	66.6	47.1
RovCol-T (Cai et al., 2023)	88M	741G	50.6	68.9	54.9	43.8	66.7	47.4
Swin-S (Liu et al., 2021)	107M	838G	51.8	70.4	56.3	44.7	67.9	48.5
RovCol-S (Cai et al., 2023)	118M	833G	52.6	71.1	56.8	45.5	68.8	49.0
Swin-B (Liu et al., 2021)	145M	982G	51.9	70.5	56.4	45.0	68.1	48.9
RovCol-B (Cai et al., 2023)	196M	988G	53.0	71.4	57.3	45.9	69.1	50.1
ConvNeXt-T	86M	741G	50.8	69.4	55.2	44.5	66.9	48.5
ConvNeXt-S	108M	827G	51.9	71.0	56.6	45.4	68.6	49.5
ConvNeXt-B	146M	964G	52.7	71.3	57.2	45.6	68.9	49.5
CEDNet-NeXt-T	87M	753G	52.5	71.4	56.8	45.9	69.0	49.7
CEDNet-NeXt-S	110M	833G	53.5	72.4	58.1	46.7	69.9	50.6
CEDNet-NeXt-B	148M	968G	53.6	72.6	57.8	46.9	70.2	51.0

2017b), Mask R-CNN (He et al., 2017), and Cascade Mask R-CNN (Cai & Vasconcelos, 2018). All training settings were same as the fine-tuning settings in Section 4.1.

**Main results.** Table 2 presents the object detection results of the CEDNet models to compare with other methods. The CEDNet models yielded significant gains over the ConvNeXt models.

Table 3: Results of semantic segmentation on the ADE20K *validation* set. The superscripts <sup>ss</sup> and <sup>ms</sup> denote single-scale and multi-scale testing. FPN was adopted as the default fusion module for methods except CEDNet. No extra fusion modules were required after the CEDNet backbone.

Method	Param.	FLOPs	Input size	mIoU <sup>ss</sup>	mIoU <sup>ms</sup>
Focal-T (Yang et al., 2021)	62M	998G	512 <sup>2</sup>	45.5	47.0
RovCol-T (Cai et al., 2023)	60M	937G	512 <sup>2</sup>	47.4	47.6
Swin-S (Liu et al., 2021)	81M	1038G	512 <sup>2</sup>	47.6	49.5
Focal-S (Yang et al., 2021)	85M	1130G	512 <sup>2</sup>	48.0	50.0
RovCol-S (Cai et al., 2023)	90M	1031G	512 <sup>2</sup>	47.9	49.0
Swin-B (Liu et al., 2021)	121M	1188G	512 <sup>2</sup>	48.1	49.7
Focal-B (Yang et al., 2021)	126M	1354G	512 <sup>2</sup>	49.0	50.5
RovCol-B (Cai et al., 2023)	122M	1169G	512 <sup>2</sup>	49.0	50.1
ConvNeXt-T (Liu et al., 2022)	60M	939G	512 <sup>2</sup>	46.0	46.7
ConvNeXt-S (Liu et al., 2022)	82M	1027G	512 <sup>2</sup>	48.7	49.6
ConvNeXt-B (Liu et al., 2022)	122M	1170G	512 <sup>2</sup>	49.1	49.9
CEDNet-NeXt-T	61M	962G	512 <sup>2</sup>	48.3	48.9
CEDNet-NeXt-S	83M	1045G	512 <sup>2</sup>	49.8	50.4
CEDNet-NeXt-B	123M	1184G	512 <sup>2</sup>	49.9	51.0

Specifically, CEDNet-NeXt-T achieved 2.2%, 2.9%, 2.8%, and 1.7% box AP improvements over its counterpart ConvNeXt-T based on the Deformable DETR, RetinaNet, Mask R-CNN, and Cascade Mask R-CNN, respectively. When scaled up to CEDNet-NeXt-S, CEDNet still outperformed its baseline ConvNeXt-S by 1.3%, 2.2%, 1.9%, and 1.6% box AP based on the four detectors.

### 4.3 INSTANCE SEGMENTATION ON COCO

**Settings.** We conducted experiments on instance segmentation with COCO 2017 (Lin et al., 2014) based on the commonly used Mask R-CNN (He et al., 2017) and Cascade Mask R-CNN (Cai & Vasconcelos, 2018) following (Liu et al., 2022; 2021). These two frameworks perform object detection and instance segmentation in a multi-task manner. All training settings were same as Section 4.1.

**Main results.** Table 2 presents the instance segmentation results (see the columns for metrics  $AP^m$ ,  $AP_{50}^m$ , and  $AP_{75}^m$ ). Based on Mask R-CNN, the models CEDNet-NeXt-T and CEDNet-NeXt-S outperformed their counterparts ConvNeXt-T and ConvNeXt-S by 1.8% and 1.2% mask AP, respectively. When applied to the more powerful Cascade Mask R-CNN, the proposed CEDNet models still yielded 1.3-1.4% mask AP gains over the baseline models. These improvements were consistent with those in object detection. When scaled up to the larger model CEDNet-NeXt-B, CEDNet achieved 46.9% mask AP based on the Cascade Mask R-CNN.

### 4.4 SEMANTIC SEGMENTATION ON ADE20K

**Settings.** We conducted experiments on semantic segmentation with the ADE20k (Zhou et al., 2017) dataset based on UperNet (Xiao et al., 2018) using the MMSegmentation (Contributors, 2020) toolboxes, and report the results on the validation set. The training settings strictly follow (Liu et al., 2022). As the data augmentation strategies used for semantic segmentation were strong enough to train the proposed CEDNet models, no extra data augmentation was introduced.

**Main results.** Table 3 presents the semantic segmentation results. Compared with the ConvNeXt models, CEDNet achieved 0.8-2.2% mIoU gains in the multi-scale test setting with different model variants, which demonstrates the effectiveness of our method in semantic segmentation.

### 4.5 ABLATION STUDIES

To better understand CEDNet, we ablated some key components and evaluated the performance in object detection based on CEDNet-NeXt-T and RetinaNet. Models in Tables 4 and 6 were pre-



Table 4: Early feature fusion.  $n_1^i, n_2^i, n_3^i$  are the number of blocks in the  $i$ -th stage.

Time	#Stage	$n_1^1, n_2^1, n_3^1$	$n_1^2, n_2^2, n_3^2$	Param	AP <sup>b</sup>
6/6	2	6, 9, 3	-	38M	40.6
5/6	2	5, 10, 5	1, 2, 1	38M	42.2
4/6	2	4, 8, 4	2, 4, 2	38M	42.4
3/6	2	3, 6, 3	3, 6, 3	38M	42.9
2/6	2	2, 4, 2	4, 8, 4	38M	<b>43.3</b>
1/6	2	1, 2, 1	5, 10, 5	38M	<b>43.3</b>
2/6	3	2, 4, 2	2, 4, 2	39M	<b>43.3</b>

Table 6: Number of stages.

$m$	$n_1, n_2, n_3$	Param	AP <sup>b</sup>
1	6, 9, 3	38M	40.6
2	3, 6, 3	38M	42.9
3	2, 4, 2	39M	<b>43.3</b>
4	1, 4, 1	39M	43.1

Table 7: Data augmentation.

Backbone	Aug.	AP <sup>b</sup>
ConvNeXt-T	Existing	45.2
ConvNeXt-T	Ours	45.4
CEDNet-NeXt-T	Existing	47.0
CEDNet-NeXt-T	Ours	<b>48.3</b>

Table 8: LR CED block.

LR block	Param	AP <sup>b</sup>
	38.5M	47.9
✓	38.6M	<b>48.3</b>

Table 5: Different token mixers. WA and DW are short for window attention and depth-wise.

Backbone	Token mixer	Param	AP <sup>b</sup>
ResNet-50	Vanilla conv $3 \times 3$	38M	41.7
CEDNet-R50-T		39M	<b>45.3</b>
Swin-T	Local WA	39M	44.9
CEDNet-Swin-T		37M	<b>47.4</b>
ConvNeXt-T	DW conv $7 \times 7$	39M	45.4
CEDNet-NeXt-T		39M	<b>48.3</b>
CSwin-T	Cross WA	32M	48.0
CEDNet-CSwin-T		33M	<b>49.5</b>

trained on ImageNet for 100 epochs and fine-tuned on COCO for 12 epochs. The other models were trained under the same settings as Section 4.1.

**Effectiveness of early feature fusion.** To explore the effectiveness of early feature fusion, we constructed several two-stage CEDNet-NeXt-T models varying in fusion time. We modulated the fusion time of each model by adjusting the computational resources allocated to each stage. All models have a similar size. Table 4 shows that the detection accuracy (AP<sup>b</sup>) gradually improved as the time for multi-scale feature fusion becomes earlier, which demonstrates that early feature fusion is beneficial for dense prediction tasks. Although the two-stage CEDNet models which allocate a proper proportion of computational resources to each stage performed well, we adopted the same configuration for all stages by default to simplify the structure design and employed three stages to achieve early feature fusion instead (the last row in Table 4).

**Effectiveness on different token mixers.** We constructed the CEDNet models with various token mixers and compared the resulting models with their counterparts (Table 5). The CEDNet models consistently surpassed their counterparts by 1.5-3.6% mAP, which underscores the generality of our CEDNet. *While CEDNet yielded better performance when utilizing the more powerful cross-window attention introduced in CSwin Transformer (Dong et al., 2022), we opted for the more representative ConvNeXt as our baseline in this work and took the  $7 \times 7$  depth-wise convolution from ConvNeXt as the default token mixer for CEDNet.*

**Different numbers of stages.** We built the CEDNet-NeXt-T models with different numbers of stages while maintaining the same configurations across stages. A model with more stages performs multi-scale feature fusion earlier. Table 6 shows that the CEDNet-NeXt-T model with three stages achieved the best detection accuracy. Intuitively, a model with more stages can fuse features more sufficiently, but more network connections may make it harder to optimize.

**Influence of data augmentation.** We compared the data augmentation strategy used by (Liu et al., 2022) and the enhanced data augmentation strategy we adopted for detection fine-tuning. Table 7 shows that the ConvNeXt models achieved similar results under both settings, but our CEDNet model exhibited notable improvements with the enhanced data augmentation. This may be because that CEDNet has a higher capacity than ConvNeXt, and the data augmentation strategy for training the ConvNeXt models are not sufficient to harness the full potential of the CEDNet models.

**Effectiveness of the LR CED block.** Table 8 shows the results of ablation experiments about the LR CED block. The model with LR CED block achieved 0.4% box AP gains over the model without LR CED block. Since the LR CED block only incorporates a lightweight dilated *depth-wise* convolution beyond the standard CED block, it introduces negligible increase in parameters (less than 1%).

## 5 CONCLUSION

We present a universal network named CEDNet for dense prediction tasks. Unlike the widely-used FPN and its variants that usually employ a lightweight fusion module to fuse multi-scale features from pre-designed classification networks, CEDNet introduces several cascade stages to learn multi-scale features. By integrating multi-scale features in the early stages, CEDNet achieves more effective feature fusion. We conducted extensive experiments on several popular dense prediction tasks. The excellent performance demonstrates the effectiveness of our method.

**Acknowledgements.** We thank Chufeng Tang, Junru Tan, Kai Li, Hang Chen, Junnan Chen for valuable discussions and feedback. This work was supported by the National Natural Science Foundation of China (Nos. 62061136001, U19B2034, 61836014) and THU-Bosch JCML center.

## REFERENCES

- Jimmy Lei Ba, Jamie Ryan Kiros, and Geoffrey E. Hinton. Layer normalization. In *arXiv:1607.06450*, 2016.
- Yuxuan Cai, Yizhuang Zhou, Qi Han, Jianjian Sun, Xiangwen Kong, Jun Li, and Xiangyu Zhang. Reversible column networks. In *International Conference on Learning Representations (ICLR)*, 2023.
- Zhaowei Cai and Nuno Vasconcelos. Cascade r-cnn: Delving into high quality object detection. In *IEEE Conference on Computer Vision and Pattern Recognition (CVPR)*, 2018.
- Kai Chen, Jiaqi Wang, Jiangmiao Pang, Yuhang Cao, Yu Xiong, Xiaoxiao Li, Shuyang Sun, Wansen Feng, Ziwei Liu, Jiarui Xu, Zheng Zhang, Dazhi Cheng, Chenchen Zhu, Tianheng Cheng, Qijie Zhao, Buyu Li, Xin Lu, Rui Zhu, Yue Wu, Jifeng Dai, Jingdong Wang, Jianping Shi, Wanli Ouyang, Chen Change Loy, and Dahua Lin. Mmdetection: Open mmlab detection toolbox and benchmark. In *Computer Research Repository*, volume abs/1906.07155, 2019.
- Liang-Chieh Chen, Yukun Zhu, George Papandreou, Florian Schroff, and Hartwig Adam. Encoder-decoder with atrous separable convolution for semantic image segmentation. In *European Conference on Computer Vision (ECCV)*, 2018.
- MMSegmentation Contributors. MMSegmentation: Openmmlab semantic segmentation toolbox and benchmark. <https://github.com/open-mmlab/mms Segmentation>, 2020.
- J. Deng, W. Dong, R. Socher, L.-J. Li, K. Li, and L. Fei-Fei. ImageNet: A large-scale hierarchical image database. In *IEEE Conference on Computer Vision and Pattern Recognition (CVPR)*, 2009.
- Xiaoyi Dong, Jianmin Bao, Dongdong Chen, Weiming Zhang, Nenghai Yu, Lu Yuan, Dong Chen, and Baining Guo. Cswin transformer: A general vision transformer backbone with cross-shaped windows. In *IEEE Conference on Computer Vision and Pattern Recognition (CVPR)*, 2022.
- Xianzhi Du, Tsung-Yi Lin, Pengchong Jin, Golnaz Ghiasi, Mingxing Tan, Yin Cui, Quoc V. Le, and Xiaodan Song. Spinenet: Learning scale-permuted backbone for recognition and localization. In *IEEE Conference on Computer Vision and Pattern Recognition (CVPR)*, 2020.
- Jiemin Fang, Lingxi Xie, Xinggang Wang, Xiaopeng Zhang, Wenyu Liu, and Qi Tian. Msg-transformer: Exchanging local spatial information by manipulating messenger tokens. In *IEEE Conference on Computer Vision and Pattern Recognition (CVPR)*, 2022.
- Golnaz Ghiasi, Tsung-Yi Lin, Ruoming Pang, and Quoc V. Le. Nas-fpn: Learning scalable feature pyramid architecture for object detection. In *IEEE Conference on Computer Vision and Pattern Recognition (CVPR)*, 2019.
- Golnaz Ghiasi, Yin Cui, Aravind Srinivas, Rui Qian, Tsung-Yi Lin, Ekin D. Cubuk, Quoc V. Le, and Barret Zoph. Simple copy-paste is a strong data augmentation method for instance segmentation. In *IEEE Conference on Computer Vision and Pattern Recognition (CVPR)*, 2021.
- Kaiming He, Xiangyu Zhang, Shaoqing Ren, and Jian Sun. Deep residual learning for image recognition. In *IEEE Conference on Computer Vision and Pattern Recognition (CVPR)*, 2016.

- Kaiming He, Georgia Gkioxari, Piotr Dollar, and Ross Girshick. Mask R-CNN. In *IEEE International Conference on Computer Vision (ICCV)*, 2017.
- Dan Hendrycks and Kevin Gimpel. Gaussian error linear units (gelus). In *arXiv:1606.08415*, 2016.
- Xiaolin Hu, Chufeng Tang, Hang Chen, Xiao Li, Jianmin Li, and Zhaoxiang Zhang. Improving image segmentation with boundary patch refinement. In *International Journal of Computer Vision*, 2022.
- Yiqi Jiang, Zhiyu Tan, Junyan Wang, Xiuyu Sun, Ming Lin, and Hao Li. Giraffedet: A heavy-neck paradigm for object detection. In *International Conference on Learning Representations (ICLR)*, 2022.
- Alex Krizhevsky, Ilya Sutskever, and Geoffrey E Hinton. Imagenet classification with deep convolutional neural networks. In *Neural Information Processing Systems (NeurIPS)*, 2012.
- Tsung-Yi Lin, Michael Maire, Serge Belongie, James Hays, Pietro Perona, Deva Ramanan, Piotr Dollár, and C. Lawrence Zitnick. Microsoft COCO: Common objects in context. In *European Conference on Computer Vision (ECCV)*, 2014.
- Tsung-Yi Lin, Piotr Dollar, Ross Girshick, Kaiming He, Bharath Hariharan, and Serge Belongie. Feature pyramid networks for object detection. In *IEEE Conference on Computer Vision and Pattern Recognition (CVPR)*, 2017a.
- Tsung-Yi Lin, Priya Goyal, Ross Girshick, Kaiming He, and Piotr Dollar. Focal loss for dense object detection. In *IEEE International Conference on Computer Vision (ICCV)*, 2017b.
- Shu Liu, Lu Qi, Haifang Qin, Jianping Shi, and Jiaya Jia. Path aggregation network for instance segmentation. In *IEEE Conference on Computer Vision and Pattern Recognition (CVPR)*, 2018.
- Yudong Liu, Yongtao Wang, Siwei Wang, Tingting Liang, Qijie Zhao, Zhi Tang, and Haibin Ling. Cbnet: A novel composite backbone network architecture for object detection. In *The Association for the Advancement of Artificial Intelligence (AAAI)*, 2020.
- Ze Liu, Yutong Lin, Yue Cao, Han Hu, Yixuan Wei, Zheng Zhang, Stephen Lin, and Baining Guo. Swin transformer: Hierarchical vision transformer using shifted windows. In *IEEE International Conference on Computer Vision (ICCV)*, 2021.
- Zhuang Liu, Hanzi Mao, Chao-Yuan Wu, Christoph Feichtenhofer, Trevor Darrell, and Saining Xie. A convnet for the 2020s. In *IEEE Conference on Computer Vision and Pattern Recognition (CVPR)*, 2022.
- Alejandro Newell, Kaiyu Yang, and Jia Deng. Stacked hourglass networks for human pose estimation. In *European Conference on Computer Vision (ECCV)*, 2016.
- Siyuan Qiao, Liang-Chieh Chen, and Alan Yuille. Detectors: Detecting objects with recursive feature pyramid and switchable atrous convolution. In *IEEE Conference on Computer Vision and Pattern Recognition (CVPR)*, 2021.
- Olaf Ronneberger, Philipp Fischer, and Thomas Brox. U-net: Convolutional networks for biomedical image segmentation. In *International Conference on Medical Image Computing and Computer Assisted Intervention (MICCAI)*, 2015.
- Karen Simonyan and Andrew Zisserman. Very deep convolutional networks for large-scale image recognition. In *International Conference on Learning Representations (ICLR)*, 2015.
- Christian Szegedy, Wei Liu, Yangqing Jia, Pierre Sermanet, Scott Reed, Dragomir Anguelov, Dumitru Erhan, Vincent Vanhoucke, and Andrew Rabinovich. Going deeper with convolutions. In *IEEE Conference on Computer Vision and Pattern Recognition (CVPR)*, 2015.
- Mingxing Tan, Ruoming Pang, and Quoc V. Le. Efficientdet: Scalable and efficient object detection. In *IEEE Conference on Computer Vision and Pattern Recognition (CVPR)*, 2020.
- Zhi Tian, Chunhua Shen, Hao Chen, and Tong He. FCOS: Fully convolutional one-stage object detection. In *IEEE International Conference on Computer Vision (ICCV)*, 2019.

- Jingdong Wang, Ke Sun, Tianheng Cheng, Borui Jiang, Chaorui Deng, Yang Zhao, Dong Liu, Yadong Mu, Mingkui Tan, Xinggang Wang, Wenyu Liu, and Bin Xiao. Deep high-resolution representation learning for visual recognition. In *IEEE transactions on pattern analysis and machine intelligence (TPAMI)*, 2019.
- Tete Xiao, Yingcheng Liu, Bolei Zhou, Yuning Jiang, and Jian Sun. Unified perceptual parsing for scene understanding. In *European Conference on Computer Vision (ECCV)*, 2018.
- Jianwei Yang, Chunyuan Li, Pengchuan Zhang, Xiyang Dai, Bin Xiao, Lu Yuan, and Jianfeng Gao. Focal self-attention for local-global interactions in vision transformers. In *Neural Information Processing Systems (NeurIPS)*, 2021.
- Jianwei Yang, Chunyuan Li, Xiyang Dai, and Jianfeng Gao. Focal modulation networks. In *Neural Information Processing Systems (NeurIPS)*, 2022.
- Gang Zhang, Xin Lu, Jingru Tan, Jianmin Li, Zhaoxiang Zhang, Quanquan Li, and Xiaolin Hu. Refinemask: Towards high-quality instance segmentation with fine-grained features. In *IEEE Conference on Computer Vision and Pattern Recognition (CVPR)*, 2021.
- Lvmin Zhang, Anyi Rao, and Maneesh Agrawala. Adding conditional control to text-to-image diffusion models. In *IEEE International Conference on Computer Vision (ICCV)*, 2023a.
- Xiaosong Zhang, Yunjie Tian, Lingxi Xie, Wei Huang, Qi Dai, Qixiang Ye, and Qi Tian. Hivit: A simpler and more efficient design of hierarchical vision transformer. In *International Conference on Learning Representations (ICLR)*, 2023b.
- Bolei Zhou, Hang Zhao, Xavier Puig, Sanja Fidler, Adela Barriuso, and Antonio Torralba. Scene parsing through ade20k dataset. In *IEEE Conference on Computer Vision and Pattern Recognition (CVPR)*, 2017.
- Xizhou Zhu, Weijie Su, Lewei Lu, Bin Li, Xiaogang Wang, and Jifeng Dai. Deformable {detr}: Deformable transformers for end-to-end object detection. In *International Conference on Learning Representations*, 2021.
- Barret Zoph and Quoc V. Le. Neural architecture search with reinforcement learning. In *International Conference on Learning Representations (ICLR)*, 2017.

Table 9: Results of image classification on the ImageNet-1K *val*. All models were trained and evaluated on 224×224 resolution with the same settings.

Method	Param.	FLOPs	Top-1 Acc.
HRNet-w32 (Wang et al., 2019)	38M	7.6G	78.4
Swin-T (Liu et al., 2021)	28M	4.4G	81.2
MSG-T (Fang et al., 2022)	25M	3.8G	82.4
FocalNet-T (Yang et al., 2022)	28M	4.5G	82.1
RovCol-T (Cai et al., 2023)	30M	4.5G	82.2
Swin-S (Liu et al., 2021)	50M	8.7G	83.1
MSG-S (Fang et al., 2022)	56M	8.4G	83.4
FocalNet-S (Yang et al., 2022)	50M	8.6G	83.4
RovCol-S (Cai et al., 2023)	60M	9.0G	83.5
Swin-B (Liu et al., 2021)	88M	15.4G	83.4
MSG-B (Fang et al., 2022)	84M	14.2G	84.0
FocalNet-B (Yang et al., 2022)	89M	15.4G	83.9
RovCol-B (Cai et al., 2023)	138M	16.6G	84.1
ConvNeXt-T (Liu et al., 2022)	29M	4.5G	82.1
ConvNeXt-S (Liu et al., 2022)	50M	8.7G	83.1
ConvNeXt-B (Liu et al., 2022)	89M	15.4G	83.8
CEDNet-NeXt-T (Hourglass-style)	34M	5.7G	82.6
CEDNet-NeXt-T (UNet-style)	34M	5.7G	82.9
CEDNet-NeXt-T (FPN-style)	34M	5.7G	83.1
CEDNet-NeXt-S (FPN-style)	55M	9.8G	83.9
CEDNet-NeXt-B (FPN-style)	95M	16.2G	84.3

## A IMAGE CLASSIFICATION ON IMAGENET-1K

Table 9 shows the results of the CEDNet models in comparison with other methods. The CEDNet models achieved better results than their counterparts, *i.e.*, the ConvNeXt models. This improvement is likely because that the pre-trained CEDNet models have slightly more parameters than their counterparts. The increased number of parameters arises from the fact that these pre-trained CEDNet models are specifically designed for downstream dense prediction tasks. In these tasks, models using CEDNet as their backbone do not need additional fusion modules, which are indispensable for their counterparts. Therefore, we allocated a few extra parameters to the CEDNet models in Table 9 to ensure that all models in subsequent dense prediction tasks have comparable size for a fair comparison (refer to the parameters and FLOPs presented in Table 1 of the paper). *Please note that the CEDNet is specifically designed for dense prediction tasks, and surpassing state-of-the-art methods in image classification is not our goal.*

## B FURTHER ANALYSIS

We analyzed why CEDNet performed better than its baselines by comparing their input gradient distributions. Specifically, we focused on the images in the COCO *val 2017* where the CEDNet models achieved the most improvements over their counterparts. We fed the selected images into the trained detectors and performed the backward process to acquire the input gradient maps of total detection loss. For each image, we define the *important region* as the region where the absolute gradient is greater than  $t$ , and  $t$  is a threshold to adjust the size of the important region.

**How to acquire the target images?** For every annotated object in an image, we first acquired the detection result with maximum IoU. If there is no matched result for a specific object, we added a virtually matched result for it and set both the IoU and confidence score of the matched result to zero. We then calculated the *detection quality score* of each annotated object by multiplying the IoU and the confidence score of the matched result. The detection quality score of an image was the average quality score of all objects in the image. Finally, we obtained the top-1000 images where the CEDNet models achieved the most improvements according to the image detection quality scores.

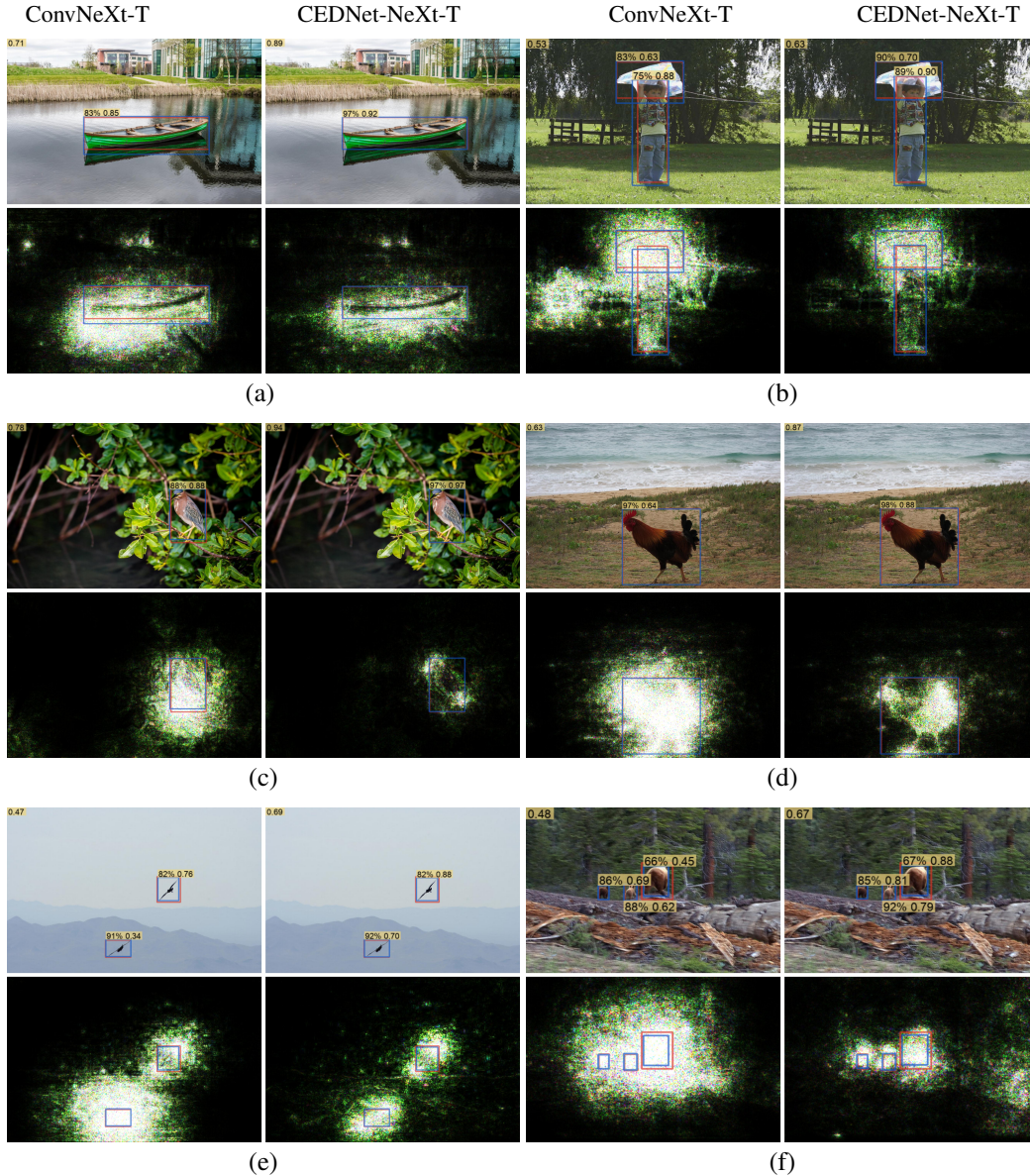


Figure 4: Detection results (top row) and input gradient maps (bottom row) of RetinaNet based on ConvNeXt-T (left column) and CEDNet-NeXt-T (right column). Red boxes represent human-annotated boxes, and blue ones indicate predicted boxes. Above each predicted box, the score pair (iou, confidence) is provided. The image detection quality score is displayed in the top left corner of each image. In the gradient maps, brighter colors signify higher gradients. Please zoom in for a clearer view.

**Results.** We compared CEDNet with ConvNeXt and Swin Transformer based on RetinaNet. Figure 4 shows that the RetinaNet with CEDNet concentrates more on objects with more discriminative boundaries and predicts more precise bounding boxes with higher confidences. In some cases (panels (d)-(f)), the IoUs of the boxes predicted by the CEDNet-based RetinaNet are close to that predicted by the ConvNeXt-based RetinaNet, but the confidences of these boxes predicted by the CEDNet-based RetinaNet are higher than that predicted by the ConvNeXt-based RetinaNet. The higher confidences of true positive predictions are more likely to lead to a higher mAP because the confidences of predicted boxes decide the ranking when calculating the precision-recall curve. In addition, we calculated the average area of important regions with different gradient thresholds on those selected images. Figure 5 shows that the average area of important regions generated from the

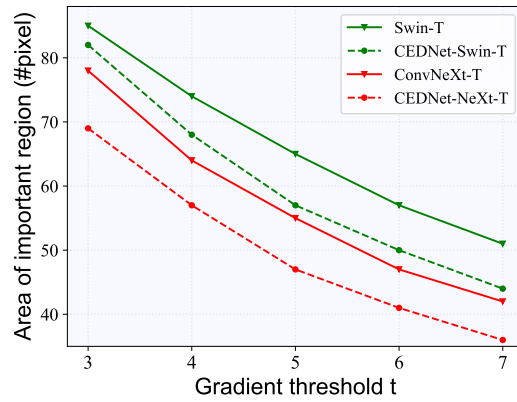


Figure 5: Comparison on the average area of *important regions* generated from RetinaNet models based on various backbones with different gradient thresholds. We normalized the values of both axes for better visualization.

CEDNet-based detectors is smaller than that generated from their counterparts, indicating that the CEDNet models concentrate on smaller regions.